Biogeosciences Discuss., 9, 701–744, 2012
www.biogeosciences-discuss.net/9/701/2012/
doi:10.5194/bgd-9-701-2012

Biogeosciences Discussions

Spatial and temporal variability in nutrients and carbon uptake during 2004 and 2005 in the eastern equatorial Pacific Ocean

A. P. Palacz and F. Chai

School of Marine Sciences, University of Maine, Aubert Hall, 04469 Orono, ME, USA

Received: 5 January 2012 – Accepted: 8 January 2012 – Published: 18 January 2012

Correspondence to: A. P. Palacz (artur.palacz@maine.edu)

Published by Copernicus Publications on behalf of the European Geosciences Union.

Abstract

The Eastern Equatorial Pacific plays a great role in the global carbon budget due to its enhanced biological productivity linked to the equatorial upwelling. However, as confirmed by the Equatorial Biocomplexity cruises in 2004 and 2005, nutrient upwelling supply varies strongly, also due to the Tropical Instability Waves. The aim of this study is to examine patterns of spatial and temporal variability in the biological uptake of NO_3, $Si(OH)_4$ and carbon in this region, and to evaluate the role of biological and physical interactions controlling these processes over seasonal and intra-seasonal time scales. Here, high resolution Pacific ROMS-CoSiNE model results are combined with in situ and remote sensing data. The results of model-data comparison reveal an excellent agreement in domain-average hydrographic and biological rate estimates, and patterns of spatio-temporal variability in primary productivity. We demonstrate for the first time that Tropical Instability Waves can be directly linked to increased NO_3 and $Si(OH)_4$ upwelling supply and enhanced nutrient and carbon uptake, in particular by large phytoplankton such as diatoms. In order to fully resolve the complexity of biological and physical interactions in the Eastern Equatorial Pacific, we recommend improving the CoSiNE model by introducing more phytoplankton groups and a variable Redfield ratio.

1 Introduction

1.1 Importance of the eastern equatorial Pacific

The Eastern Equatorial Pacific (EEP) plays a great role in the global carbon (C) cycling due to its enhanced biological productivity linked to the equatorial upwelling. Encompassing the equatorial upwelling zone (EUZ; 3° S–3° N, 140–90° W), the EEP provides the largest natural oceanic source of CO_2 into the atmosphere at about 0.7 to 1.0 Pg C yr^{-1} (Tans et al., 1990; Takahashi et al., 2003), decreasing to 0.2 to

BGD
9, 701–744, 2012

0.4 Pg C yr^{-1} during strong El Niño years (Ishii et al., 2009). Primary productivity (PP) in the EEP is significantly greater than in any other open ocean province, with an average value of 642 mg C m^2 d^{-1} (Pennington et al., 2006). Due to the large areal extent of the EEP, its new production is estimated to account for 18 % of global new production (Chavez and Toggweiler, 1995). Despite the very high biological productivity, the EEP is a so-called "High Nitrate, Low Chlorophyll" (HNLC) region, with excess nitrate (NO_3) and unexpectedly low chlorophyll-*a* (Chl) concentrations in the surface waters (Minas et al., 1986; Dugdale and Wilkerson, 1998). The EEP is characterized by a strong zonal and meridional gradient in nutrients (iron (Fe), nitrogen (N), silicon (Si)) and Chl concentrations (Jiang et al., 2003; Pennington et al., 2006; Kaupp et al., 2011). The eastward shoaling Equatorial Undercurrent (EUC) provides the largest source of these nutrients in the EEP, mostly through upwelling of deeper waters (Palacz et al., 2011). However, the supply of these elements into the EEP surface waters is variable and hence constitutes an important factor in regulating local phytoplankton production (Wells et al., 1999; Christian et al., 2002; Slemons et al., 2009; Gorgues et al., 2010).

The Equatorial Biocomplexity (EB) project was a recent attempt to elucidate the role of biological and physical interactions in controlling nutrient dynamics in the EEP. Two cruises conducted in December 2004 (EB04) and September 2005 (EB05) aimed at investigating ecological and chemical processes associated with, and responsible for, the HNLC conditions in the EEP (Nelson and Landry, 2011). Data collected from the EB04 and EB05 cruises was unprecedented with regard to the rate measurements, the spatial area covered and the vertical profiles obtained (Nelson and Landry, 2011). In comparison to previous investigations in this region (e.g., EqPac, CLIVAR P16N cruise), the results of EB studies revealed large variability in nutrient concentrations as well as uptake rates, and suggested that the relative roles of different regulatory mechanisms can vary significantly both spatially and temporarily in the EEP (Nelson and Landry, 2011). The 2004 and 2005 cruises showed relatively little difference in the hydrography (Strutton et al., 2011) because they took place during similar seasonal and El Niño conditions. However, remote sensing and Tropical Atmosphere Ocean

BGD
9, 701–744, 2012

(TAO) buoy time series observations demonstrate that the EEP responds to changes in coupled atmosphere-ocean circulation associated with seasons (Philander et al., 1987; Murray et al., 1994), tropical instability waves (TIWs) (Foley et al., 1997), and the El Niño Southern Oscillation (ENSO) (Wang and Fiedler, 2006, and references therein).

1.2 Previous carbon and nutrient uptake estimates

There have been few directly measured rates of phytoplankton nitrate uptake (ρNO_3) (Dugdale et al., 1992; McCarthy et al., 1996; Rodier and Le Borgne, 1997; Raimbault et al., 1999), silicic acid uptake ($\rho Si(OH)_4$) (Dam et al., 1995; McCarthy et al., 1996; Blain et al., 1997; Leynaert et al., 2001), and PP (Barber et al., 1996) in the EEP prior to the EB cruises. In order to resolve the dynamics of biogeochemical cycling of nutrients and biological productivity in the EEP, Dugdale and Wilkerson (1998) developed a biological model of the EUZ, which was based on the idea of Si-limitation in this region. Their model was later combined with the N-based model of Chai et al. (1996) to create the one-dimensional Carbon, Silicon, Nitrogen Ecosystem (CoSiNE) model (Chai et al., 2002). Combining the CoSiNE model with three-dimensional physical models such as the NCAR climate ocean model (NCOM) (Gent et al., 1998) or the Regional Ocean Modeling System (ROMS) model (Wang and Chao, 2004), resulted in the first comprehensive NO_3, $Si(OH)_4$, Fe and C budgets for the EEP (Jiang et al., 2003; Palacz et al., 2011). Additionally, size-fractionated nutrient uptake rates from the EB04 and EB05 cruises were previously compared with the 50 km Pacific ROMS-CoSiNE results and revealed good agreement in mean equatorial ρNO_3 and ammonia uptake (ρNH_4), particulate organic N and f-ratios (Dugdale et al., 2007).

The EB04 and EB05 cruises provided the much needed in situ measurements, which can be used to evaluate the CoSiNE model results, such as nutrients and their supplies, nutrient uptake rates, phytoplankton biomass and composition, and specific growth and grazing rates. Comparing zooplankton grazing rates (Taylor et al., 2011) with phytoplankton growth rates (Selph et al., 2011), Landry et al. (2011) concluded that the

BGD
9, 701–744, 2012

HNLC surface waters of the EEP exhibit a balance of growth and grazing processes, thus placing a constraint on the magnitude of phytoplankton biomass and C export flux. However, they also pointed at the possible local and episodic nature of C export in the EEP, likely linked to TIW activity. They suggested that fluxes must be calculated at a higher spatial and temporal resolution to answer the question of how important production, recycling and export fluxes are in the overall nutrient and C budgets.

1.3 Objectives

The aim of this study is to examine patterns of spatial and temporal variability in the biological uptake of NO_3, $Si(OH)_4$ and C in the EEP, and to evaluate the role of biological and physical interactions controlling these processes. We present the results of an integrated effort to address some of the questions formulated but left unanswered by the EB project which only revealed a snapshot view of the changes in nutrient dynamics and biological productivity. Three-day averaged model results allow for a two year, near-continuous record of coincident mesoscale (12.5 km resolution) changes in circulation and biological production. Such detailed spatial and temporal analysis of changes in biological processes in the EEP has previously only been performed on surface Chl distribution using remote sensing data (e.g., Chavez et al., 1999; Strutton et al., 2001; Ryan et al., 2006; Strutton et al., 2011). By combining model results with the remote sensing estimates of biological production and the findings of the EB cruises, we investigate the dynamics of the processes controlling nutrient cycling and C production in the EEP in an integrated fashion, consistent in time and space.

2 Model and data

2.1 Coupled physical-biogeochemical model

Model calculations are performed using the biogeochemical model CoSiNE (Chai et al., 2002; Dugdale et al., 2002) coupled with the ROMS circulation model. This coupled

BGD
9, 701–744, 2012

model was first configured for the Pacific Ocean domain (45° S–65° N, 99° E–70° W) with realistic geometry and topography by Wang and Chao (2004) at a 50 km spatial resolution, and later at an increased resolution of 12.5 km by Xiu and Chai (2010). Initialized with climatological temperature and salinity from the World Ocean Atlas (WOA) 2001 (Ocean Climate Laboratory National Oceanographic Data Center, 2002), the Pacific ROMS model has been forced with the climatological NCEP/NCAR reanalysis of air-sea fluxes (Kalnay et al., 1996) for several decades in order to reach quasi equilibrium. The model is then integrated for the period of 1991 to 2010 forced with daily air-sea fluxes of heat and fresh water from the NCEP/NCAR reanalysis (Kalnay et al., 1996). The heat flux is derived from short- and long-wave radiations and sensible and latent heat fluxes calculated using the bulk formula with prescribed air temperature and relative humidity. The multiple satellite blended daily sea wind with a resolution of 0.25° (Zhang et al., 2006) is used to calculate the surface wind stress based on the bulk formula of Large and Pond (1982). Detailed physical and biological model configuration can be found in Liu and Chai (2009), Chai et al. (2009), and Xiu and Chai (2010).

Here, we analyze the results from a coupled physical-biogeochemical model at the 12.5 km spatial and three-day temporal resolution that is capable of resolving mesoscale features in physical circulation (Xiu et al., 2010) and biogeochemical fluxes (Xiu et al., 2011; Xiu and Chai, 2011). Principal CoSiNE equations describing biological processes and which differ from the ones in Chai et al. (2002), are listed in Appendix A.

The results are a combination of on-line and off-line model calculations – an approach that was validated in Palacz et al. (2011) and which allowed us to optimize the model performance specifically in the EEP region. In this study, we use on-line calculated three-day averaged net short-wave radiation flux (which is converted to light field to calculate biological production), temperature and nutrient concentration fields. These variables provide input for off-line calculated vertical light profiles, phytoplankton and zooplankton biomass, specific growth rates, nutrient uptake rates and grazing. Our model results include two groups of phytoplankton, small and large phytoplankton, and two groups of zooplankton, micro- and mesozooplankton. Size-fractionated

BGD
9, 701–744, 2012

phytoplankton ρNO_3, $\rho Si(OH)_4$ and ρNH_4 are calculated explicitly. Total N uptake ($\rho NO_3 + \rho NH_4$) is converted into C units using a fixed Redfield ratio of 6.6 to estimate PP.

Off-line calculations offer several advantages for this modeling study. First, they are computationally less costly and more time efficient. By performing more model runs we are able to test different model configurations and parameter values in order to simulate the EEP conditions best. For example, we distinguish between using daily-averaged and diurnal cycle of light as an energy source for phytoplankton growth. Second, we conduct series of sensitivity studies to find an optimum set of biological parameters, including $\rho Si(OH)_4$ and ρNH_4 half-saturation constants, Si:N uptake ratio or zooplankton grazing rates. While many parameters in the biological model are the same as in Chai et al. (2002), others, listed in Table 1, are modified based either on the findings of the EB project or are derived from model sensitivity runs. Although the off-line calculations do not account for advection in phytoplankton and zooplankton biomass, considering that turnover of phytoplankton biomass is comparable to the three-day period during which two on-line variables (surface light and nutrients) are updated, the modeled distribution of phytoplankton biomass is not likely to be affected significantly by this limitation. Growth rates and nutrient uptake rates are calculated off-line every hour and later averaged into three-day estimates.

In this study, model domain is equal to the EEP box delineated between 140–110° W and 1° S–1° N to match the area most heavily sampled during both EB cruises, and at the same time, to confine the box to the upwelling dominated EUZ. Hence, our calculations are consistent and directly comparable with budget calculations performed by Jiang et al. (2003) and more recently by Palacz et al. (2011).

2.2 Cruise data

Evaluation of the 12.5 km Pacific ROMS-CoSiNE nutrient cycling results is based on comparison with corresponding measurements conducted during the two EB cruises aboard the R/V Revelle, EB04 in December 2004 and EB05 in September 2005.

BGD
9, 701–744, 2012

Details of station locations and hydrographic conditions from both cruises can be found in Strutton et al. (2011). Sampling and data analysis methods of ρNO_3 and ρNH_4 measurements are described in Dugdale et al. (2007) and Parker et al. (2011). Krause et al. (2011) give a detailed procedure for calculating $\rho Si(OH)_4$ rates, while Balch et al. (2011) provide information on estimating total community and size-fractionated C fixation rates.

2.3 Statistical analysis

The skill of Pacific ROMS-CoSiNE model is assessed using comparisons with data collected in situ during EB cruises. Apart from mean and variability estimates, we calculate model bias (B; representing the difference between the means of the two fields), and the centered pattern root mean square difference ($RMSD_{cp}$; equivalent to an unbiased RMSD representing the differences in the variability of the two fields). Combining B and $RMSD_{cp}$ we obtain the total RMSD ($RMSD_{tot}$) which provides a valuable overall comparison of model and data fields (Campbell et al., 2002; Friedrichs et al., 2009).

Model-data comparison of nutrient uptake rates is illustrated by means of a target diagram (Jolliff et al., 2009). Target diagrams are used to visualize B, $RMSD_{cp}$ and $RMSD_{tot}$ on a single plot. On the target diagram, these statistical metrics are normalized by standard deviation of the data (σ_d). On this plot, normalized B is on the y-axis and normalized $RMSD_{cp}$ is on the x-axis. Concentric circles represent normalized $RMSD_{tot}$ isolines with the solid circle representing the normalized deviation of the data. If model $RMSD_{tot}$ exceeds the standard deviation of observations, i.e. $RMSD_{tot} > 1$, then the model is showing less skill than does the mean of observations.

3 Results and discussion

In this section, we describe patterns of variability in model phytoplankton nutrient and C uptake in the EEP during 2004–2005. First, we verify the capability and skill of the

BGD
9, 701–744, 2012

Pacific ROMS-CoSiNE model to reproduce the hydrographic conditions encountered during the EB04 and EB05 cruises. Second, we compare the EB cruise and modeled biological environment of the EEP, including phytoplankton growth and nutrient uptake rates, biomass and species composition. Third, we present the two-year time series of nutrient and C uptake rates. Fourth, we present patterns of spatio-temporal variability in nutrient and C uptake rates as well as the corresponding upwelling supply rates. We also discuss the origin of observed patterns of variability in the context of satellite estimates of PP in the 2004–2005 period.

3.1 Hydrographic conditions

In Table 2 we summarize the mean and standard deviation of the EEP box averaged model and EB data hydrography. In Fig. 1, a more detailed comparison at individual stations using scatter plots verifies the model skill in simulating zonal and vertical gradients in temperature (T), dissolved oxygen (O_2), NO_3 and $Si(OH)_4$.

There is a wide range of T in the top 150 m of the water column (Fig. 1a), suggesting a steep thermocline that is indicative of a strong cold water upwelling in the EUZ. There is a high and statistically significant linear correlation between in situ measured and modeled T during December 2004 ($r = 0.97$, $p < 0.01$) and September 2005 ($r = 0.91$, $p < 0.01$). A small but consistent negative bias indicates that the model tends to slightly underestimate T with respect to both EB04 (bias of $-1.53\,^{\circ}C$) and EB05 (bias of $-2.71\,^{\circ}C$) observations. The bias is larger in the lower range of T, corresponding to shallower depths (Fig. 1a). Nevertheless, this bias, describing the difference between the means of two datasets, does not contribute much to $RMSD_{tot}$. The $RMSD_{cp}$, or the unbiased RMSD, which is used to assess the differences in variability, is relatively low for T (0.95 and $1.35\,^{\circ}C$ in 2004 and 2005, respectively). This good overall relationship is also evident in the domain-average mean and standard deviation model and data estimates (Table 2).

The model also does well when simulating the distribution of O_2 (Fig. 1b), a proxy for both upwelling of deep waters and biological remineralization activity. There is a high

BGD
9, 701–744, 2012

correlation between model and data, especially in September 2005 ($r = 0.93$, $p < 0.01$). The model simulates the observed variability very well, with a small difference in amplitude of variability between the two years (Fig. 1b and Table 2). A consistent positive bias present in the model is more visible than in the case of T (compare Fig. 1b with 1a), but shows little statistical difference between 2004 and 2005 (29.0 vs. 29.3 mg O_2 m^{-3}). Figure 1b reveals that the largest bias occurs at mid O_2 range.

NO_3 and $Si(OH)_4$ concentrations are compared in Fig. 1c,d, respectively. Both relationships are very highly correlated and statistically significant at the 99 % level ($r > 0.90$). We note that model NO_3 is overestimated in its lower values (at the surface) but underestimated it its higher values (below the euphotic zone). This is likely related to the bias in T identified in Fig. 1a. The ratio of model to data standard deviations (σ_m/σ_d) of NO_3 reveals that the model also underestimates the amplitude of variability, more so in September 2005 than in December 2004 (0.42 vs. 0.77). Table 2 confirms that while the mean model and data fields are very similar, the model NO_3 variability (standard deviation) is underestimated relative to other hydrographic factors.

Small positive model bias in surface NO_3 and low NO_3 variability is unlikely to create a positive bias in phytoplankton new production. This is because of predominant Si-limitation of large phytoplankton, maintained by a consistently low ratio of surface $Si(OH)_4$ to NO_3 (compare Fig. 1c and d), as well as a high NH_4 inhibition of ρNO_3 in small phytoplankton (ψ_{S1} in Table 1). In the model it is assumed that $Si(OH)_4$ availability plays the main role in controlling large phytoplankton growth and new production because they share the functional properties of diatoms.

A very good model-data comparison of $Si(OH)_4$ and other hydrographic parameters (Table 2 and Fig. 1), provides confidence in Pacific ROMS-CoSiNE's ability to simulate the characteristic LSiHNLC conditions of the EEP region, and justifies the use of our model approach to perform the biological rate calculations described in the next sections.

BGD
9, 701–744, 2012

3.2 Nutrient and C uptake rates

In Table 3 we summarize the mean monthly-averaged model PP (equivalent to phytoplankton uptake of C) and nutrient uptake rates (ρNO_3, ρNH_4 and $\rho Si(OH)_4$), integrated over the top 75 m depth (using the standard trapezoidal method). We compare them with similar estimates from the EB04 and EB05 cruises (Balch et al., 2011; Parker et al., 2011; Krause et al., 2011). Here, standard deviations correspond to the scale of zonal and meridional variability modeled or observed within the EEP box. The model does an excellent job in capturing the mean state of all biological rates in the EEP domain, but in general performs better in December 2004. The only visible large discrepancy between model and data occurs for ρNH_4 during September 2005. There is a consistent positive bias associated with $\rho Si(OH)_4$ that originates from the fact that all large phytoplankton in the model take up $Si(OH)_4$, while in the field, diatoms comprise only a fraction of that population (Parker et al., 2011; Taylor et al., 2011). Nevertheless, most model rate estimates are within a factor of two from the mean in situ measurements. Such a good box-average agreement is the basis for positive model performance evaluation.

Additionally, in Fig. 2 we use a target diagram to illustrate the normalized biased and unbiased statistical metrics used to compare ROMS-CoSiNE and EB macronutrient and C uptake rates. We conclude that the spatial variability in uptake rates is modeled reasonably well, with the exception of $\rho Si(OH)_4$ that was shown to be overestimated for reasons discussed above. It is clear that there are large year to year discrepancies in the model bias. On the other hand the unbiased $RMSD_{cp}$ shows no such trend, and remains relatively low for both uptake rate estimates.

Results shown in Fig. 2 also reveal a certain paradox by which the model provides a consistently good representation of PP over the two year sampling periods, but less satisfying results of ρNO_3 and ρNH_4 in 2005 than in 2004. If total C uptake by phytoplankton is linked to the uptake of total N by means of a constant Redfield ratio (PP = Redfield ratio $\times$ ($\rho NO_3 + \rho NH_4$)) as it is done in the ROMS-CoSiNE model, then

BGD
9, 701–744, 2012

we would expect no discrepancy in the model bias and variability of N and C uptake between the two time periods. C uptake during EB was measured independently (Balch et al., 2011) and is prone to a different sampling error than ρNO_3 and ρNH_4 (Parker et al., 2011). However, both methods of calculating uptake rates have been performed side by side in the Equatorial Pacific during previous cruises and are unlikely to carry a measurement error large enough to explain this difference. Thus, it is likely that the model assumption of a constant Redfield ratio needs to be reevaluated in order to more accurately capture the dynamics of C and nutrient uptake rates in the EEP.

In order to fully inspect the model skill in describing the phytoplankton nutrient uptake dynamics in the EEP, we further verify how the model captures the mean phytoplankton specific growth rate (μ) and phytoplankton biomass (S), the product of which determines the total nutrient uptake rates.

3.3 Specific growth rates and biomass

The analysis of EEP box mean μ and S is particularly useful in illustrating why the total N and C uptake rates are well modeled under December 2004 but less so under September 2005 conditions (Fig. 3 and Table 3). The mean total phytoplankton μ, calculated on the basis of a seawater dilution method (Selph et al., 2011), equals $0.53 \pm 0.11\,d^{-1}$ in December 2004 and is well matched and only slightly underestimated by the model mean equal to $0.45 \pm 0.03\,d^{-1}$ (Table 4). However, in September 2005, the model overestimates μ despite of displaying much lower standard deviation associated with spatial variability (Table 4). At the same time, total phytoplankton biomass, defined as total amount of Chl pigment in cells $> 0.45\,\mu m$ in diameter, was estimated at $26.5 \pm 3.4\,mg\,Chl\,m^{-2}$ during EB04 (Balch et al., 2011). This is in excellent agreement with the modeled $28.4 \pm 4.6\,mg\,Chl\,m^{-2}$. The comparison is even better in September 2005 when the model S matches perfectly both in terms of the mean and variability (Table 4).

The conclusions derived from these results shed more light on the year-to-year discrepancy in model performance in simulating total nutrient and C uptake rates. It appears that the model does an excellent job in capturing the mean state of total

BGD
9, 701–744, 2012

phytoplankton biological production described by PP, total μ and S. However, when looking at ρNO_3, ρNH_4 and $\rho Si(OH)_4$ we need to consider what the species composition of the phytoplankton community looks like. The model, which only uses a simple two phytoplankton group setup and assumes that all large phytoplankton have the same functional behavior as diatoms, does not simulate all phytoplankton growth dynamics well as revealed by the discrepancy in 2004 and 2005 ρNH_4, or the consistent positive bias in $\rho Si(OH)_4$. In the following section we explore the possible role of this limitation in preventing the model from fully resolving the patterns of variability in biological production in the EEP.

3.4 Phytoplankton species composition

The numerous studies integrated within the EB project reveal a very dynamic phytoplankton community with relative abundances of several autotrophic functional groups shifting on small spatial and temporal scales (Selph et al., 2011; Stukel et al., 2011; Taylor et al., 2011). One of the issues addressed by the EB project was the role of diatoms in regulating the productivity of the HNLC waters in the EEP. While the total and relative abundance of individual phytoplankton groups was investigated using flow cytometry pigment analysis (Taylor et al., 2011), their contribution to nutrient and C uptake was based on size-fractionated measurements. Integrating results from these two different approaches allowed for an indirect estimate of the role of diatoms in nutrient cycling in the EEP.

Parker et al. (2011) speculated that the role of diatoms in total ρNO_3 could be several times higher than their biomass contribution ($< 10\,\%$). At the same time, they pointed at the importance of accounting for large dinoflagellates which obtain their N from both mixotrophy and nitrate uptake. Large dinoflagellates have a big share in new production while constituting for much of the larger size fraction of phytoplankton biomass. Since the CoSiNE model only takes into account two functional types of phytoplankton, we cannot distinguish between diatoms and dinoflagellates in the large phytoplankton size fraction. However, through a comparison of large phytoplankton cell biomass obtained

BGD
9, 701–744, 2012

from size-fractionated Chl measurements (Balch et al., 2011) and pigment-specific diatom concentration (Taylor et al., 2011), we can comment on the role of diatoms in nutrient uptake relative to their biomass, and place this discussion in the context of the disparate September 2005 N, Si and C flux estimates discussed above.

While diatoms comprise on average only 6.5 % of the total autotrophic community in the study periods (Taylor et al., 2011), Parker et al. (2011) documented that diatoms make up between 13 and 37 % of the total phytoplankton community. However, at several biological "hotspots" along the equator, they constitute between 3 and 45 % of the >5 µm phytoplankton size group, in December 2004 and September 2005, respectively (Parker et al., 2011). These hotspots, associated with strong upwelling at the leading or trailing edge of a TIW, also strongly affect ρNO_3 and $\rho Si(OH)_4$ variability along the equator (Parker et al., 2011; Krause et al., 2011). In the model, large phytoplankton biomass oscillates between 24 and 44 % of total biomass across the entire 2004–2005 period but is on average equal to 42 % during the two months when EB cruises took place. This estimate is higher than 6.5 % diatom biomass contribution measured in the field, and also an overestimate with respect to the 20–30 % contribution of the >3 µm phytoplankton biomass reported by Balch et al. (2011).

It appears that the current version of the CoSiNE model cannot simulate a lower large phytoplankton biomass while maintaining diatom's large contribution to ρNO_3. On the other hand, large (>5 µm) dinoflagellates, which do not have a Si-requirement for growth and thus do not obscure the $\rho Si(OH)_4$ model-data comparison, can have a large contribution to total ρNO_3 whenever their N demand is not satisfied by phagotrophy (Stukel et al., 2011). Assuming that diatoms compete for both NO_3 and NH_4, as it is also assumed in the model, Parker et al. (2011) estimated that dinoflagellates account on average for 55 % of ρNO_3 in the >5 µm fraction. It seems that further improvement in the model calculations cannot take place without introducing new phytoplankton functional groups, such as the dinoflagellates.

In order to place this discussion back into the context of total nutrient and C uptake rates, we refer to the role of diatoms in new and primary production. The EB cruises

BGD
9, 701–744, 2012

reported that diatoms on average would account for 45 % of ρNO_3 (Parker et al., 2011). This is in excellent agreement with the model large phytoplankton ρNO_3 of 48 % in December 2004, and 50 % in September 2005. Diatom contribution to PP in the model is 40 % in December 2004 and 37 % in September 2005. Landry et al. (2011) calculated that large eukaryotic phytoplankton constituted between 15 and 62 % of primary production in the EEP, with diatoms contributing on average 18 % of total autotrophic production. This indicates minor fluctuations in the otherwise overestimated role of model diatoms in PP variability in the EEP.

Another means of evaluating the role of diatoms in new production is to calculate their f-ratios. In the model, diatoms have an average f-ratio of 0.39 and 0.36 in December 2004 and September 2005, respectively. This is in very good agreement with the $>5\,\mu m$ size-fractionated f-ratio from EB04 and EB05 (Table 5). Slightly higher model values are to be expected if lack of mixotrophic (with much lower f-ratios) dinoflagellates in the model is considered. Unfortunately, there are no diatom specific f-ratio estimates from either of the EB cruises. Comparison of the modeled small phytoplankton and total autotrophic community f-ratios reveals a similarly good agreement with the EB data (Table 5).

In order to understand the discrepancy between the modeled and the observed nutrient and C uptake rates, it is important to mention the significant differences in phytoplankton composition reported during EB cruises. In September 2005, contribution of *Prochloroccocus* towards total autotrophic biomass increased by more than twofold (Taylor et al., 2011). These small cells rely on NH_4 as their principal source of N for growth, and their elevated biomass enhanced ρNH_4 more than twofold during EB05 (Table 3; Parker et al., 2011). ρNO_3 by large phytoplankton increased as well (Parker et al., 2011) but without a concomitant elevation in $\rho Si(OH)_4$ (Krause et al., 2011). Parker et al. (2011) demonstrated that in Decemeber 2004 ρNO_3 by cells $>5\,\mu m$ was equal or greater than the estimated diatom demand for N. In September 2005, it was much lower than the diatom demand, suggesting an increase in relative contribution of large dinoflagellates (that do not take up Si) to ρNO_3. At the same time, in situ

BGD
9, 701–744, 2012

observations reported only a small change in the EEP mean PP (Table 3); (Balch et al., 2011).

Therefore, we conclude that while the CoSiNE model simulates the overall phytoplankton nutrient uptake dynamics well, its size-fractionated nutrient uptake is not always adequate to represent the interaction between shifts in phytoplankton species composition and nutrient and C uptake rates. Future improvements in the model design will require a greater diversification of phytoplankton functional groups in order to better represent the short-term, spatially diverse changes in phytoplankton community structure observed in the EEP (Selph et al., 2011; Stukel et al., 2011; Taylor et al., 2011), as recommended by Parker et al. (2011).

3.5 Patterns of temporal variability

Figure 3 shows the time distribution of depth-integrated (0–75 m) and area-averaged (1° S–1° N, 140–110° W) PP, ρNO_3, $\rho Si(OH)_4$ and ρNH_4 from January 2004 to December 2005. Superimposed on the model time series are the cruise-averaged biological uptake rates measured in situ. A one standard deviation range of both model and cruise estimates illustrates the zonal variation range in the biological rates between 140° W and 110° W. The well aligned model and cruise estimates of PP and ρNO_3 especially (Fig. 3a,c) reflect the good agreement presented in Table 3.

Figure 3a reveals that the EEP-averaged PP oscillates strongly on intraseasonal time scales, with visible low frequency modulations of the variability amplitude. The 2004–2005 mean PP equals 54.7 mmol C m^{-2} d^{-1}, with a minimum of 37.8 and a maximum of 68.3 mmol C m^{-2} d^{-1}. Mean ρNO_3 is estimated at 2.49 mmol N m^{-2} d^{-1} but varies by more than a factor of three across the time period, from a minimum of 1.19 to a maximum of 4.12 mmol N m^{-2} d^{-1} (Fig. 3b). $\rho Si(OH)_4$ has a minimum value of 2.07 mmol Si m^{-2} d^{-1} and a maximum of 5.37 mmol Si m^{-2} d^{-1}. Mean $\rho Si(OH)_4$ equals 3.65 mmol Si m^{-2} d^{-1}.

BGD
9, 701–744, 2012

In Fig. 3d we also present the model time series of ρNH_4. The September 2005 mismatch between mean model and data value, attributed to a twofold increase in *Prochloroccocus* abundance (Parker et al., 2011; Taylor et al., 2011), is now better explained by a relatively low ρNH_4 variability in the EEP across the two year period. The 2004–2005 model mean ρNH_4 is 5.81 mmol N m^{-2} d^{-1}, with the maximum domain average uptake rate of 7.66 mmol N m^{-2} d^{-1}. ρNH_4 data presented by Parker et al. (2011) are in the range of values reported from the JGOFS EqPac studies (Pena et al., 1994; McCarthy et al., 1996). However, Parker et al. (2011) admit that their EB ρNH_4 measurements had limitations originating from the need for ^{15}N enrichment to stimulate any ρNH_4 under very low ambient NH_4 concentrations in the collected water samples. Such an interpretation of overestimated in situ ρNH_4 is consistent with the results of the theoretical calculations of C uptake derived from total N using a 6.6–7.3 Redfield ratio range conversion. The observed high ρNH_4 would require C uptake much higher than the PP measured in situ (Balch et al., 2011), which however is in good agreement with our model PP estimates (Figs. 2 and 3, Table 3). It is difficult to constrain ρNH_4 in the model because of two reasons. First, rapid turnover time of NH_4, on an order of one hour, makes modeling NH_4 dynamics very difficult. Second, the major source of NH_4 is from regeneration processes that depend on zooplankton biomass, another biological factor that is difficult to constrain and capture in the model. Regardless of the error associated with the ρNH_4 estimates, in situ and model alike, availability of NH_4 is not expected to limit phytoplankton growth and thus is not a deterministic factor in regulating C cycling in the EEP.

Results presented in Fig. 3 address an important issue of how much vital information about temporal variability in phytoplankton and nutrient dynamics remains unaccounted for when comparing results from consecutive cruises substantially separated in time. While the TAO buoy array (http://www.pmel.noaa.gov/tao/) provides time series of physical oceanographic and atmospheric data, there is no direct way of evaluating patterns of variability in biological process, other than remotely-measured surface Chl, and their interactions with changes in the physical circulation. In Fig. 4 we compare the

BGD
9, 701–744, 2012

modeled three-day average PP with the remote-sensing-derived eight-day composite net primary production (NPP) from two Vertically Generalized Production Models (VGPMs), standard and Eppley-modified, and the updated C-based Production Model (CbPM) (http://www.science.oregonstate.edu/ocean.productivity/). NPP from VGPMs is a function of Chl, available light, and the photosynthetic efficiency (Behrenfeld and Falkowski, 1997). The CbPM relates NPP to phytoplankton C biomass and μ by retrieving information about particle backscatter and absorption (Westberry et al., 2008).

All time series in Fig. 4 come from depth-integrated and area-averaged PP between January 2004 and December 2005. The VGPM and CbPM offer the only sound reference frame for evaluating the pattern and amplitude of temporal variability of the ROMS-CoSiNE estimated PP. In general, the mean and variability of the modeled PP are in the middle of the range of values obtained from the three satellite-derived NPP estimates. While the two VGPMs are visibly lower in both their mean and range of variability, the amplitude of CbPM variability is close in line with the modeled one, though its mean value is higher than that of ROMS-CoSiNE.

Based on the modeled high amplitude and frequency of variability in both PP and nutrient uptake (Figs. 3 and 4), we expect that distribution of biological rates is affected by individual TIW events, occurring every four to five weeks on average. Figure 5 demonstrates that our ROMS-CoSiNE model is capable of capturing the TIW dynamics in the EEP. The latitude-longitude surface plots of SST and Chl reveal a passing TIW that disturbs the SST field via enhanced upwelling (colder SST), and which promotes a significant response in biological productivity (higher Chl).

Although there are no studies that examine the effect of passing TIWs on the distribution of satellite-measured PP in the EEP, studies of surface distribution of Chl have shown that this proxy for phytoplankton biomass, which is related to C production, is strongly regulated by these fast moving, westward propagating TIWs (e.g., Chelton et al., 2000; Strutton et al., 2001, 2011; Ryan et al., 2006).

Furthermore, we suspect that if the large and high-frequency temporal variability is also reflected in the spatial distribution of biological productivity within the EEP region,

BGD
9, 701–744, 2012

then looking at the area-averaged time series of nutrient and C uptake rates might mask some important patterns of spatial variability occurring within the EEP domain. Therefore, we also examine patterns of zonal variability in nutrient and C uptake rates and how they may differ in time over the 2004–2005 period.

3.6 Patterns of spatio-temporal variability

We use the Hovmöller diagrams to illustrate patterns of spatio-temporal variability in the nutrient and C uptake rates. We present results from two regions: (1) averaged over the upwelling dominated 1° S–1° N meridional domain, (2) and averaged over the 1–3° N meridional domain which includes the area most affected by passing TIWs in the EEP (Evans et al., 2009). Figure 6 shows the scale and pattern of variability in depth-integrated nutrient uptake rates from the two regions. As expected, ρNH_4 dominates in both the mean and variability compared to ρNO_3 and $\rho Si(OH)_4$. In the 1° S–1° N region (top panels of Fig. 6), the distribution of nutrient uptake rates is very patchy. While there are no distinguishable patterns in ρNO_3, ρNH_4 displays periods of very elevated uptake interrupted by short periods of very little biological activity. In early fall in both 2004 and 2005, ρNH_4 is consistently very high all along the equator. Although the timing coincides with the maximum in TIW intensity, no frontal features can be associated with elevated regenerated production. However, when looking at the distribution of $\rho Si(OH)_4$, fronts of elevated uptake propagating from east to west are very pronounced. Consistently with ρNH_4, maximum $\rho Si(OH)_4$ takes place during fall of each year. By estimating the time it would take such a front to cross from 110° W to 140° W, we conclude that these features are most likely caused by passing TIWs.

TIW signature is even stronger in the spatio-temporal distribution of nutrient uptake rates in the 1–3° N region (bottom panels of Fig. 6). Being further away from the equator and the area of maximum upwelling, biological fluxes are in general lower than at the equator. Yet, they exhibit much higher variability associated with episodically very high nutrient uptake events. Lines of elevated $\rho Si(OH)_4$ uptake are well matched in time and space with those identified in the along-equatorial region. Moreover, these

BGD
9, 701–744, 2012

frontal features associated with elevated $\rho Si(OH)_4$ are now easily identified in the ρNH_4 distribution. This suggests that in the absence of strong background recycling of N, the effect of passing TIWs can not only enhance the new but also fuel the regenerated biological production in the EEP.

The strongest TIW signature is captured in the modeled distribution of $\rho Si(OH)_4$ (Fig. 6b,e). Here, we see fast-moving waves passing through the EEP at regular 4–5 week intervals, reflected in bands of elevated $\rho Si(OH)_4$ very closely resembling bands of elevated surface Chl concentrations observed from space by Strutton et al. (2001) or Ryan et al. (2006). In between the strong TIW seasons there are periods of very low $\rho Si(OH)_4$ recorded, as in March and April 2005. These are likely linked with the passage of Kelvin waves. We speculate that the effect of Kelvin waves is to decrease diatom activity and biological uptake of Si by decreasing the upwelling supply of $Si(OH)_4$ into the euphotic zone. Under the same conditions, small phytoplankton are affected less as they rely on NH_4 and NO_3 for growth. Both these nutrients are not limiting in the EEP surface waters.

In order to verify these speculations, we plot the time-longitude distribution of NO_3 and $Si(OH)_4$ positive upwelling flux into the top 75 m water column together with the surface concentrations of these nutrients in the TIW-dominated, 1–3° N domain (Fig. 7). It appears that the prominent wave-like features are also distinguished in the upwelling flux distribution, in the $Si(OH)_4$ flux in particular. Furthermore, it can be noticed that the elevated supply of this growth-limiting nutrient coincides with area and time of elevated surface $Si(OH)_4$ concentration (Fig. 7d). Even though this relationship is less pronounced in the distribution of ρNO_3, the effect of passing TIWs on the supply of NO_3 (Fig. 7a) and its surface concentration (Fig. 7c) is nevertheless visible. Estimates of wave speed and frequency of the frontal features identified in Fig. 7 also confirm that they are likely the result of intense TIW activity, especially in the fall and early winter in both 2004 and 2005.

Finally, we analyze the spatio-temporal distribution of PP in both the 1° S–1° N and 1–3° N regions. In Fig. 8 we compare the model and satellite depth-integrated and

BGD
9, 701–744, 2012

meridional average PP. Based on the model-satellite time series comparison shown in Fig. 4, we choose the standard VGPM version of the satellite PP estimate to evaluate the model spatio-temporal patterns of variability. First, we notice areas of elevated PP in both the model and satellite data in the early fall of both 2004 and 2005. Highest PP values are found in the eastern side of the region but lines of elevated production can be seen to frequently propagate westward. Second, we see long periods of extremely low PP all over the EEP domain, similarly in the model and satellite result (e.g., March and April 2005). These features match well with time and location of depressed nutrient uptake likely caused by a strong Kelvin wave (Fig. 6). The wave-like or frontal features in PP, associated with passing TIWs, are much more pronounced in the 1–3° N region, as expected. Although model PP is on average higher than estimated using remote sensing, similarity in the patterns is striking. Considering that TIW signature is strongest in the distribution of $\rho Si(OH)_4$ and appears in the distribution of PP as well, we can assume that the role of large phytoplankton, or diatoms in particular, might be critical to determining the overall distribution of depth-integrated PP. Even though our model overestimates the diatom contribution to biomass, this does not seem to affect model PP variability strongly, especially considering the excellent model-satellite agreement in PP distribution seen in Fig. 8.

However, there are some minor but important discrepancies between model and satellite PP patterns of variability. For instance, elevated PP in early fall lasts for a few weeks longer in the model result. This is also reflected in the mismatch between model and satellite PP time series compared in Fig. 4. We were able to attribute these discrepancies in PP to a relatively higher small phytoplankton population seen in the model during October and November 2005, also reported during the EB05 cruise (Parker et al., 2011). Blooms of small phytoplankton, as indicated by high *Prochloroccocus* biomass during EB05, typically occur below the surface (Selph et al., 2011) and it is possible that the satellite VGPM model of PP does not take this into account. Even though the VGPM model attempts to estimate depth-integrated and not only surface PP, its algorithm is inherently dependent on the estimates of surface optical properties

BGD
9, 701–744, 2012

predominantly. We suggest that further model and satellite comparisons are necessary to fully evaluate the role of subsurface processes on biological productivity in the entire euphotic zone.

We consider our results an important validation of the ROMS-CoSiNE model capability to accurately represent spatial and temporal patterns of variability in biological productivity in the EEP. Although there is no direct means of validating the model pattern of nutrient uptake rate distribution, the consistency between nutrient upwelling supply flux, surface nutrient concentration and PP patterns of variability indicates a very strong connection between TIW activity and nutrient uptake rates in the EEP. This study potentially provides key evidence for the water column link between physical and biological variability in the EEP so far mostly identified for surface processes (e.g., Strutton et al., 2001; Ryan et al., 2006).

Furthermore, our results confirm that bottom-up regulation through variable nutrient supply significantly impacts the productivity of the EEP and can explain the dominant features in the observed spatial and temporal variability. Nonetheless, a much more complex interaction between biological and physical processes likely takes place in the EEP. Top-down control, though not investigated in this study, might be equally modulated by the TIW and Kelvin wave activity but may also act on different time scales.

4 Conclusions

In this study we demonstrate that the 12.5 km ROMS-CoSiNE model can simulate nutrient dynamics and biological productivity in the EEP, described by the EB04 and EB05 cruises. The model accurately represents the mean and variability in hydrographic conditions, including temperature, NO_3 and $Si(OH)_4$, and O_2. Modeled PPs of 53.1 ± 5.5 and 64.1 ± 6.2 mmol C m^{-2} d^{-1} agree extremely well with EEP box averages of 62.4 ± 9.2 and 59.3 ± 18.6 mmol C m^{-2} d^{-1} measured in December 2004 and September 2005, respectively. Modeled ρNO_3 in December 2004 and September 2005 are 2.46 ± 0.63 and 2.67 ± 0.76 mmol N m^{-2} d^{-1}, which agree within a factor of two with

BGD
9, 701–744, 2012

EB04 and EB04 cruise measurements of 3.59 ± 1.32 and 4.17 ± 1.82 mmol N m^{-2} d^{-1}. Measured $\rho Si(OH)_4$ values of 1.70 ± 0.56 and 1.23 ± 0.61 mmol Si m^{-2} d^{-1} are overestimated by modeled 3.18 ± 1.02 and 3.58 ± 1.25 mmol Si m^{-2} d^{-1} in December 2004 and September 2005, respectively, due to lack of functional diversity among modeled large phytoplankton. We demonstrate that the Pacific ROMS-CoSiNE model can accurately simulate mean phytoplankton specific growth rates, with the modeled two-year mean of 0.45 d^{-1} matching closely with cruise average of 0.48 d^{-1}. Two-year mean depth-integrated phytoplankton biomass is 28.9 mg Chl m^{-2} in the model, very close to the corresponding cruise estimate of 29.5 mg Chl m^{-2}. Station by station comparisons provide a source of model evaluation in a statistical sense only. Lack of data assimilation prevents us from accurately constraining physical conditions in the model. Thus, modeled TIWs do not correspond exactly to those observed during the EB cruises. Nevertheless, it is important to note that the model range of variability in nutrient uptake rate, controlled by changes in the physical environment, matches extremely well with that observed in situ.

Our modeled time series of nutrient uptake rates provide a nearly-continuous record of temporal variability in nutrient dynamics and biological productivity. These results complement the scarce cruise measurements and provide a much needed reference for estimating 2004–2005 mean conditions and seasonal variability in the EEP.

Our findings point at the important role of TIWs in controlling patterns of spatial and temporal variability in nutrient, especially Si, dynamics in the EEP. It appears that TIWs passing across the EEP domain enhance $\rho Si(OH)_4$ significantly, indicating a strong response of the diatom population to perturbed Si supply conditions. While the observed phenomena are short-lived, they reveal the importance of TIWs in the context of nutrient growth limitation and frequent but likely ephemeral changes in phytoplankton species composition in the EEP. Our results provide first direct evidence that TIWs can alter the state of nutrient limitation to a large degree by supplying significant amounts of $Si(OH)_4$ causing a rapid and strong response in large phytoplankton growth and biomass. Future studies that examine the role of TIWs in changing the supply and

BGD
9, 701–744, 2012

phytoplankton uptake of iron explicitly will also help estimate the degree of co-limitation of these two elements.

Through a careful model-data comparison we also provide recommendations for how the biological CoSiNE model can be improved to better simulate nutrient dynamics and biological productivity in the EEP. Firstly, we recommend incorporating new phytoplankton functional groups into the model design, such as mixotrophic dinoflagellates. Their lack in the current model configuration may explain the observed station by station discrepancies and markedly overestimated mean $\rho Si(OH)_4$. Future development in this direction is likely to improve the model skill in representing patterns of phytoplankton productivity in response to changes in nutrient supply and uptake.

Secondly, the observed mismatch in N and C uptake by phytoplankton cannot be overcome unless a dynamic C : Chl ratio is introduced. Under the assumption of a constant C : Chl ratio, we often cannot link changes in phytoplankton biomass with patterns of variability in PP. It is particularly important to understand how these interactions alter in response to TIWs and other physical phenomena that control nutrient supply in the EEP. Thirdly, it is necessary to remove the constraint of a fixed Redfield ratio. We suspect that a dynamic N to C uptake ratio would increase the flexibility of biological production responses to changes in phytoplankton community and nutrient dynamics, especially evident during passage of TIWs, and on longer time scales, Kelvin waves.

Fourthly, the data collected from the EB04 and EB05 cruises was unprecedented with regard to the key biological rate measurements, which provide constrains on models and point to directions for improvement. When comparing observations with model results directly (i.e. matching time and space), data assimilation is necessary, which will match model physical conditions with real ocean conditions. Continued remote sensing and in situ observations of ocean physical conditions should be incorporated through data assimilation into physical-biogeochemical modeling.

BGD
9, 701–744, 2012

Appendix A

Principal CoSiNE nutrient uptake equations

A1 Small phytoplankton

$$\rho NO_3 = \mu S1_{max} \frac{NO_3}{K_{S1\_NO_3} + NO_3} e^{-\psi_{S1} NH_4} (1 - e^{(-a/(\mu S1_{max}))I}) S1 \quad \text{(A1)}$$

$$\rho NH_4 = \mu S1_{max} \frac{NH_4}{K_{S1\_NH_4} + NH_4} \left(1 - e^{(-a/(\mu S1_{max}))I}\right) S1 \quad \text{(A2)}$$

I is the vertical profile of light; a is the initial slope of the P–I curve equal to 0.025. For explanations of other symbols see Table 1.

A2 Large phytoplankton

$$\rho NO_3 = \mu S2_{max} \times MIN\left(\frac{NO_3}{K_{S2\_NO_3} + NO_3}, \frac{Si(OH)_4}{K_{Si(OH)_4} + Si(OH)_4}\right) \times \ldots$$
$$\times e^{-\psi_{S2} NH_4} (1 - e^{(-a/(\mu S2_{max}))I}) S2 \quad \text{(A3)}$$

$$\rho Si(OH)_4 = \mu S2_{max} \times MIN\left(\frac{NO_3}{K_{S2\_NO_3} + NO_3}, \frac{Si(OH)_4}{K_{Si(OH)_4} + Si(OH)_4}\right) \times \ldots$$
$$\times e^{-\psi_{S2} NH_4} (1 - e^{(-a/(\mu S2_{max}))I}) S2 \quad \text{(A4)}$$

$$\rho NH_4 = \mu S2_{max} \times MIN\left(\frac{NO_3}{K_{S2\_NO_3} + NO_3}, \frac{Si(OH)_4}{K_{Si(OH)_4} + Si(OH)_4}\right) \times \ldots$$
$$\times (1 - e^{-\psi_{S2} NH_4})(1 - e^{(-a/(\mu S2_{max}))I}) S2 \quad \text{(A5)}$$

BGD
9, 701–744, 2012

Acknowledgements. The authors would like to thank Huijie Xue, Mary Jane Perry, Mark Wells, Peter Strutton, Wiley Evans, Andy Thomas and Emmanuel Boss for their valuable comments on the manuscript. We are grateful to Lei Shi and Peng Xiu for assistance in processing the model data. This research was supported by a NASA grant (NNX09AU39G) and NSF (OCE-0961345) to F. Chai. We thank Yi Chao and his group at JPL/NASA for setting up the original Pacific-ROMS model configurations.

References

Balch, W. M., Poulton, A. J., Drapeau, D. T., Bowler, B. C., Windecker, L. A., and Booth, E. S.: Zonal and meridional patterns of phytoplankton biomass and carbon fixation in the Equatorial Pacific Ocean, between 110 degrees W and 140 degrees W, Deep-Sea Res. Pt. II, 58, 400–416, doi:10.1016/j.dsr2.2010.08.004, 2011. 708, 711, 712, 714, 716, 717, 734, 735

Barber, R., Sanderson, M., Lindley, S., Chai, F., Newton, J., Trees, C., Foley, D., and Chavez, F.: Primary productivity and its regulation in the Equatorial Pacific during and following the 1991–1992 El Nino, Deep-Sea Res. Pt. II, 43, 933–969, 1996. 704

Behrenfeld, M. and Falkowski, P.: Photosynthetic rates derived from satellite-based chlorophyll concentration, Limnol. Oceanogr., 42, 1–20, 1997. 718, 744

Blain, S., Leynaert, A., Treguer, P., Chretiennot-Dinet, M. J., and Rodier, M.: Biomass, growth rates and limitation of Equatorial Pacific diatoms, Deep-Sea Res. Pt. I, 44, 1255–1275, 1997. 704

Campbell, J., Antoine, D., Armstrong, R., Arrigo, K., Balch, W., Barber, R., Behrenfeld, M., Bidigare, R., Bishop, J., Carr, M. E., Esaias, W., Falkowski, P., Hoepffner, N., Iverson, R., Kiefer, D., Lohrenz, S., Marra, J., Morel, A., Ryan, J., Vedernikov, V., Waters, K., Yentsch, C., and Yoder, J.: Comparison of algorithms for estimating ocean primary production from surface chlorophyll, temperature, and irradiance, Global Biogeochem. Cy., 16, 1035–1050, 2002. 708

Chai, F., Lindley, S. T., and Barber, R. T.: Origin and maintenance of a high nitrate condition in the Equatorial Pacific, Deep-Sea Res. Pt. II, 43, 1031–1064, 1996. 704

Chai, F., Dugdale, R., Peng, T.-H., Wilkerson, F., and Barber, R.: One-dimensional ecosystem model of the Equatorial Pacific upwelling system. Part I: Model development and silicon and nitrogen cycle, Deep-Sea Res. Pt. II, 49, 2713–2745, 2002. 704, 705, 706, 707, 732

BGD

9, 701–744, 2012

Chai, F., Liu, G. M., Xue, H. J., Shi, L., Chao, Y., Tseng, C. M., Chou, W. C., and Liu, K. K.: Seasonal and interannual variability of carbon cycle in South China Sea: a three-dimensional physical-biogeochemical modeling study, J. Oceanogr., 65, 703–720, 2009. 706

Chavez, F. and Toggweiler, J.: Physical estimates of global new production: the upwelling contribution, in: Upwelling in the Ocean: Modern Processes and Ancient Records, edited by: Summerhayes, C., Emeis, K.-C., Angel, M., Smith, R., and Zeitschel, B., Wiley, Chichester, 313–320, 1995. 703

Chavez, F., Strutton, P., Friederich, G., Feely, R., Feldman, G., Foley, D., and McPhaden, M.: Response of the Equatorial Pacific Ocean to the 1997–1998 El Nino, Science, 286, 2126–2131, 1999. 705

Chelton, D., Wentz, F., Gentemann, C., de Szoeke, R., and Schlax, M.: Satellite microwave SST observations of transequatorial tropical instability waves, Geophys. Res. Lett., 27, 1239–1242, 2000. 718

Christian, J., Verschell, M., Murtugudde, R., Busalacchi, A., and McClain, C.: Biogeochemical modelling of the tropical Pacific Ocean. II: Iron biogeochemistry, Deep-Sea Res. Pt. II, 49, 545–565, 2002. 703

Dam, H. G., Zhang, X. S., Butler, M., and Roman, M. R.: Mesozooplankton grazing and metabolism at the equator in the Central Pacific – implications for carbon and nitrogen fluxes, Deep-Sea Res. Pt. II, 42, 735–756, 1995. 704

Dugdale, R. C. and Wilkerson, F. P.: Silicate regulation of new production in the Equatorial Pacific upwelling, Nature, 391, 270–273, 1998. 703, 704

Dugdale, R. C., Wilkerson, F. P., Barber, R. T., and Chavez, F. P.: Estimating new production in the Equatorial Pacific-Ocean at 150-degrees-W, J. Geophys. Res.-Oceans, 97, 681–686, 1992. 704

Dugdale, R. C., Barber, R. T., Chai, F., Peng, T. H., and Wilkerson, F. P.: One-dimensional ecosystem model of the Equatorial Pacific upwelling system. Part II: Sensitivity analysis and comparison with JGOFS EqPac data, Deep-Sea Res. Pt. II, 49, 2747–2768, 2002. 705

Dugdale, R. C., Wilkerson, F. P., Chai, F., and Feely, R.: Size-fractionated nitrogen uptake measurements in the Equatorial Pacific and confirmation of the low Si-high-nitrate low-chlorophyll condition, Global Biogeochem. Cy., 21, GB2005, doi:10.1029/2006GB002722, 2007. 704, 708

Evans, W., Strutton, P. G., and Chavez, F. P.: Impact of tropical instability waves on nutrient and chlorophyll distributions in the Equatorial Pacific, Deep-Sea Res. Pt. I, 56, 178–188, 2009.

BGD
9, 701–744, 2012

719
Foley, D., Dickey, T., McPhaden, M., Bidigare, R., Lewis, M., Barber, R., Lindley, S., Garside, C., Manov, D., and McNeil, J.: Longwaves and primary productivity variations in the Equatorial Pacific at 0 degrees, 140 degrees W, Deep-Sea Res. Pt. II, 44, 1801–1826, 1997. 704
Friedrichs, M. A. M., Carr, M.-E., Barber, R. T., Scardi, M., Antoine, D., Armstrong, R. A., Asanuma, I., Behrenfeld, M. J., Buitenhuis, E. T., Chai, F., Christian, J. R., Ciotti, A. M., Doney, S. C., Dowell, M., Dunne, J., Gentili, B., Gregg, W., Hoepffner, N., Ishizaka, J., Kameda, T., Lima, I., Marra, J., Melin, F., Moore, J. K., Morel, A., O'Malley, R. T., O'Reilly, J., Saba, V. S., Schmeltz, M., Smyth, T. J., Tjiputra, J., Waters, K., Westberry, T. K., and Winguth, A.: Assessing the uncertainties of model estimates of primary productivity in the tropical Pacific Ocean, J. Mar. Syst., 76, 113–133, 2009. 708
Gent, P. R., Bryan, F. O., Danabasoglu, G., Doney, S. C., Holland, W. R., Large, W. G., and McWilliams, J. C.: The NCAR Climate System Model global ocean component, J. Climate, 11, 1287–1306, 1998. 704
Gorgues, T., Menkes, C., Slemons, L., Aumont, O., Dandonneau, Y., Radenac, M. H., Alvain, S., and Moulin, C.: Revisiting the La Nina 1998 phytoplankton blooms in the Equatorial Pacific, Deep-Sea Res. Pt. I, 57, 567–576, 2010. 703
Ishii, M., Inoue, H. Y., Midorikawa, T., Saito, S., Tokieda, T., Sasano, D., Nakadate, A., Nemoto, K., Metzl, N., Wong, C. S., and Feely, R. A.: Spatial variability and decadal trend of the oceanic CO_2 in the Western equatorial Pacific warm/fresh water, Deep-Sea Res. Pt. II, 56, 591–606, 2009. 703
Jiang, M. S., Chai, F., Dugdale, R. C., Wilkerson, F. P., Peng, T. H., and Barber, R. T.: A nitrate and silicate budget in the Equatorial Pacific Ocean: a coupled physical-biological model study, Deep-Sea Res. Pt. II, 50, 2971–2996, 2003. 703, 704, 707
Jolliff, J. K., Kindle, J. C., Shulman, I., Penta, B., Friedrichs, M. A. M., Helber, R., and Arnone, R. A.: Summary diagrams for coupled hydrodynamic-ecosystem model skill assessment, J. Mar. Syst., 76, 64–82, 2009. 708
Kalnay, E., Kanamitsu, M., Kistler, R., Collins, W., Deaven, D., Gandin, L., Iredell, M., Saha, S., White, G., Woollen, J., Zhu, Y., Chelliah, M., Ebisuzaki, W., Higgins, W., Janowiak, J., Mo, K. C., Ropelewski, C., Wang, J., Leetmaa, A., Reynolds, R., Jenne, R., and Joseph, D.: The NCEP/NCAR 40-year reanalysis project, B. Am. Meteorol. Soc., 77, 437–471, 1996. 706
Kaupp, L. J., Measures, C. I., Selph, K. E., and Mackenzie, F. T.: The distribution of dissolved

BGD
9, 701–744, 2012

Fe and Al in the upper waters of the Eastern Equatorial Pacific, Deep-Sea Res. Pt. II, 58, 296–310, doi:10.1016/j.dsr2.2010.08.009, 2011. 703

Krause, J. W., Nelson, D. M., and Brzezinski, M. A.: Biogenic silica production and the diatom contribution to primary production and nitrate uptake in the Eastern Equatorial Pacific Ocean, Deep-Sea Res. Pt. II, 58, 434–448, doi:10.1016/j.dsr2.2010.08.010, 2011. 708, 711, 714, 715, 734

Landry, M. R., Selph, K. E., Taylor, A. G., Decima, M., Balch, W. M., and Bidigare, R. R.: Phytoplankton growth, grazing and production balances in the HNLC Equatorial Pacific, Deep-Sea Res. Pt. II, 58, 524–535, doi:10.1016/j.dsr2.2010.08.011, 2011. 704, 715

Large, W. G. and Pond, S.: Sensible and latent heat flux measurements over the ocean, J. Phys. Oceanogr., 12, 464–482, 1982. 706

Leynaert, A., Treguer, P., Lancelot, C., and Rodier, M.: Silicon limitation of biogenic silica production in the Equatorial Pacific, Deep-Sea Res. Pt. I, 48, 639–660, 2001. 704

Liu, G. and Chai, F.: Seasonal and interannual variability of primary and export production in the South China Sea: a three-dimensional physical-biogeochemical model study, Ices J. Mar. Sci., 66, 420–431, 2009. 706

McCarthy, J. J., Garside, C., Nevins, J. L., and Barber, R. T.: New production along 140° W in the Equatorial Pacific during and following the 1992 El Niño event, Deep-Sea Res. Pt. II, 43, 1065–1093, 1996. 704, 717

Minas, H., Minas, M., and Packard, T.: Productivity in upwelling areas deduced from hydrographic and chemical fields, Limnol. Oceanogr., 31, 1182–1206, 1986. 703

Murray, J. W., Barber, R. T., Roman, M. R., Bacon, M. P., and Feely, R. A.: Physical and biological-controls on carbon cycling in the Equatorial Pacific, Science, 266, 58–65, 1994. 704

Nelson, D. M. and Landry, M. R.: Regulation of phytoplankton production and upper-ocean biogeochemistry in the Eastern Equatorial Pacific: Introduction to results of the equatorial biocomplexity project, Deep-Sea Res. Pt. II, 58, 277–283, doi:10.1016/j.dsr2.2010.08.001, 2011. 703

Palacz, A. P., Chai, F., Dugdale, R. C., and Measures, C. I.: Estimating iron and aluminum removal rates in the Eastern Equatorial Pacific Ocean using a box model approach, Deep-Sea Res. Pt. II, 58, 311–324, doi:10.1016/j.dsr2.2010.08.012, 2011. 703, 704, 706, 707

Parker, A. E., Wilkerson, F. P., Dugdale, R. C., Marchi, A. M., Hogue, V. E., Landry, M. R., and Taylor, A. G.: Spatial patterns of nitrogen uptake and phytoplankton in the equatorial

BGD
9, 701–744, 2012

upwelling zone (110 degrees W–140 degrees W) during 2004 and 2005, Deep-Sea Res. Pt. II, 58, 417–433, doi:10.1016/j.dsr2.2010.08.013, 2011. 708, 711, 712, 713, 714, 715, 716, 717, 721, 734, 736

Pena, M., Lewis, M., and Cullen, J.: New production in the warm waters of the tropical Pacific Ocean, J. Geophys. Res.-Oceans, 99, 14255–14268, 1994. 717

Pennington, J. T., Mahoney, K. L., Kuwahara, V. S., Kolber, D. D., Calienes, R., and Chavez, F. P.: Primary production in the Eastern Tropical Pacific: a review, Progr. Oceanogr., 69, 285–317, 2006. 703

Philander, S., Hurlin, W., and Seigel, A.: Simulation of the seasonal cycle of the Tropical Pacific Ocean, J. Phys. Oceanogr., 17, 1986–2002, 1987. 704

Raimbault, P., Slawyk, G., Boudjellal, B., Coatanoan, C., Conan, P., Coste, B., Garcia, N., Moutin, T., and Pujo-Pay, M.: Carbon and nitrogen uptake and export in the Equatorial Pacific at 150 degrees W: Evidence of an efficient regenerated production cycle, J. Geophys. Res.-Oceans, 104, 3341–3356, 1999. 704

Rodier, M. and Le Borgne, R.: Export flux of particles at the equator in the Western and Central Pacific ocean, Deep-Sea Res. Pt. II, 44, 2085–2113, 1997. 704

Ryan, J. P., Ueki, I., Chao, Y., Zhang, H., Polito, P. S., and Chavez, F. P.: Western Pacific modulation of large phytoplankton blooms in the central and Eastern Equatorial Pacific, J. Geophys. Res.-Biogeo., 111, 2006. 705, 718, 720, 722

Selph, K. E., Landry, M. R., Taylor, A. G., Yang, E.-J., Measures, C. I., Yang, J., Stukel, M. R., Christensen, S., and Bidigare, R. R.: Spatially-resolved taxon-specific phytoplankton production and grazing dynamics in relation to iron distributions in the Equatorial Pacific between 110 and 140 degrees W, Deep-Sea Res. Pt. II, 58, 358–377, doi:10.1016/j.dsr2.2010.08.014, 2011. 704, 712, 713, 716, 721, 735

Slemons, L., Gorgues, T., Aumont, O., Menkes, C., and Murray, J. W.: Biogeochemical impact of a model western iron source in the Pacific Equatorial Undercurrent, Deep-Sea Res. Pt. I, 56, 2115–2128, 2009. 703

Strutton, P. G., Ryan, J. P., and Chavez, F. P.: Enhanced chlorophyll associated with tropical instability waves in the Equatorial Pacific, Geophys. Res. Lett., 28, 2005–2008, 2001. 705, 718, 720, 722

Strutton, P. G., Palacz, A. P., Dugdale, R. C., Chai, F., Marchi, A., Parker, A. E., Hogue, V., and Wilkerson, F. P.: The impact of Equatorial Pacific tropical instability waves on hydrography and nutrients: 2004–2005, Deep-Sea Res. Pt. II, 58, 284–295,

BGD
9, 701–744, 2012

doi:10.1016/j.dsr2.2010.08.015, 2011. 703, 705, 708, 718
Stukel, M. R., Landry, M. R., and Selph, K. E.: Nanoplankton mixotrophy in the Eastern Equatorial Pacific, Deep-Sea Res. Pt. II, 58, 378–386, doi:10.1016/j.dsr2.2010.08.016, 2011. 713, 714, 716
Takahashi, T., Sutherland, S., Feely, R., and Cosca, C.: Decadal variation of the surface water PCO2 in the western and central Equatorial Pacific, Science, 302, 852–856, 2003. 702
Tans, P. P., Fung, I. Y., and Takahashi, T.: Observational constrainsts on the global atmospheric CO_2 budget, Science, 247, 1431–1438, 1990. 702
Taylor, A. G., Landry, M. R., Selph, K. E., and Yang, E. J.: Biomass, size structure and depth distributions of the microbial community in the Eastern Equatorial Pacific, Deep-Sea Res. Pt. II, 58, 342–357, doi:10.1016/j.dsr2.2010.08.017, 2011. 704, 711, 713, 714, 715, 716, 717
Wang, C. Z. and Fiedler, P. C.: ENSO variability and the Eastern tropical Pacific: A review, Progr. Oceanogr., 69, 239–266, 2006. 704
Wang, X. C. and Chao, Y.: Simulated Sea Surface Salinity variability in the tropical Pacific, Geophys. Res. Lett., 31, 4, 2004. 704, 706
Wells, M. L., Vallis, G. K., and Silver, E. A.: Tectonic processes in Papua New Guinea and past productivity in the Eastern Equatorial Pacific Ocean, Nature, 398, 601–604, 1999. 703
Westberry, T., Behrenfeld, M. J., Siegel, D. A., and Boss, E.: Carbon-based primary productivity modeling with vertically resolved photoacclimation, Global Biogeochem. Cy., 22, 2008. 718
Xiu, P. and Chai, F.: Modeling the effects of size on patch dynamics of an inert tracer, Ocean Sci., 6, 413-421, doi:10.5194/os-6-413-2010, 2010. 706
Xiu, P. and Chai, F.: Modeled biogeochemical responses to mesoscale eddies in the South China Sea, J. Geophys. Res., 116, C10006, doi:10.1029/2010JC006800, 2011. 706
Xiu, P., Chai, F., Shi, L., Xue, H. J., and Chao, Y.: A census of eddy activities in the South China Sea during 1993–2007, J. Geophys. Res.-Oceans, 115, C03012, doi:10.1029/2009JC005657, 2010. 706
Xiu, P., Palacz, A. P., Chai, F., Roy, E. G., and Wells, M. L.: Iron flux induced by Haida eddies in the Gulf of Alaska, Geophys. Res. Lett., 38, L13607, doi:10.1029/2011GL047946, 2011. 706
Zhang, H. M., Bates, J. J., and Reynolds, R. W.: Assessment of composite global sampling: Sea surface wind speed, Geophys. Res. Lett., 33, L17714, doi:10.1029/2006GL027086, 2006. 706

BGD
9, 701–744, 2012

Table 1. Optimized CoSiNE model parameters. Key model parameters used in this study are compared with the early CoSiNE model parameterization applied by Chai et al. (2002).

CoSiNE model parameter	Symbol	This study	Chai et al. (2002)	Unit
Light	I	Diurnal cycle	Diurnal cycle	$W\,m^{-2}$
NH_4 inhibition for small phyto.	Ψ_{S1}	10.00	5.59	$(mmol\,m^{-2})^{-1}$
NH_4 inhibition for large phyto.	Ψ_{S2}	4.00	5.59	$(mmol\,m^{-2})^{-1}$
Half-saturation for ρNH_4 by small phyto.	$K_{S1\_NH_4}$	0.10	0.05	$mmol\,m^{-2}$
Half-saturation for ρNH_4 by large phyto.	$K_{S2\_NH_4}$	None	1.00	$mmol\,m^{-2}$
Half-saturation for ρNO_3 by small phyto.	$K_{S1\_NO_3}$	0.50	0.50	$mmol\,m^{-2}$
Half-saturation for ρNO_3 by large phyto.	$K_{S2\_NO_3}$	1.00	0.50	$mmol\,m^{-2}$
Half-saturation for $\rho Si(OH)_4$	$K_{Si(OH)_4}$	3.50	3.00	$mmol\,m^{-2}$
Large phyto. Si : N uptake ratio	Si : N	Dynamic > 1	1.00	–
Max specific growth rate of small phyto.	$\mu S1_{max}$	2.00	2.00	d^{-1}
Max specific growth rate of large phyto.	$\mu S2_{max}$	2.50	3.00	d^{-1}

BGD
9, 701–744, 2012

Table 2. The model-data comparison of domain-averaged hydrographic conditions during 2004–2005. T, O_2, NO_3 and $Si(OH)_4$ are compared for the periods December 2004 and September 2005.

Source	T (°C)		O_2 (mg O_2 m^{-3})		NO_3 (mmol N m^{-3})		$Si(OH)_4$ (mmol Si m^{-3})	
	Dec 2004	Sep 2005	Dec 2004	Sep 2005	Dec 2004	Sep 2005	Dec 2004	Sep 2005
EB data	23.1 ± 3.29	22.0 ± 4.14	161 ± 27.9	148 ± 34.6	9.62 ± 4.18	11.4 ± 7.05	5.04 ± 3.09	6.15 ± 3.07
Model	21.6 ± 2.76	20.5 ± 2.52	190 ± 28.2	177 ± 37.2	10.3 ± 3.21	11.4 ± 2.97	6.68 ± 3.48	7.64 ± 3.20

BGD
9, 701–744, 2012

Table 3. The model-data comparison of nutrient and C uptake rates during 2004–2005. Results are area-averaged and depth-integrated. Mean and standard deviation come from the along-equatorial profiles between 140° W and 110° W. PP data from Balch et al. (2011), ρNO_3 and ρNH_4 from Parker et al. (2011), and $\rho Si(OH)_4$ from Krause et al. (2011).

Source	PP (mmol C m^{-2} d^{-1})		ρNO_3 (mmol N m^{-2} d^{-1})		$\rho Si(OH)_4$ (mmol Si m^{-2} d^{-1})		ρNH_4 (mmol N m^{-2} d^{-1})	
	Dec 2004	Sep 2005	Dec 2004	Sep 2005	Dec 2004	Sep 2005	Dec 2004	Sep 2005
EB data	62.4 ± 9.2	59.3 ± 18.6	3.59 ± 1.32	4.17 ± 1.82	1.70 ± 0.56	1.23 ± 0.61	7.94 ± 5.22	17.1 ± 3.7
Model	53.1 ± 5.5	64.1 ± 6.2	2.46 ± 0.63	2.67 ± 0.76	3.18 ± 1.02	3.58 ± 1.25	5.58 ± 0.88	7.05 ± 0.78

BGD
9, 701–744, 2012

Table 4. The model-data comparison of phytoplankton specific growth rate and biomass in the EEP. Results are domain-averaged over the 1° S–1° N and 140–110° W region. Cruise specific growth rates come from Selph et al. (2011) and biomass estimates from Balch et al. (2011).

Source	Specific growth rate (d^{-1})		Total phytoplankton biomass (mg Chl m^{-2})	
	Dec 2004	Sep 2005	Dec 2004	Sep 2005
EB data	0.53 ± 0.11	0.39 ± 0.11	26.5 ± 3.4	32.4 ± 5.1
Model	0.45 ± 0.03	0.48 ± 0.03	28.4 ± 4.6	32.1 ± 4.9

BGD
9, 701–744, 2012

Table 5. The model-data comparison of domain-averaged f-ratios during 2004–2005. Total phytoplankton f-ratios are compared with size-fractionated estimates. Cruise f-ratios were calculated by Parker et al. (2011).

Source	Small phytoplankton		Large phytoplankton		Total phytoplankton	
	Dec 2004	Sep 2005	Dec 2004	Sep 2005	Dec 2004	Sep 2005
EB data	0.38	0.10	0.34	0.33	0.28	0.16
Model	0.25	0.22	0.39	0.36	0.31	0.27

BGD
9, 701–744, 2012

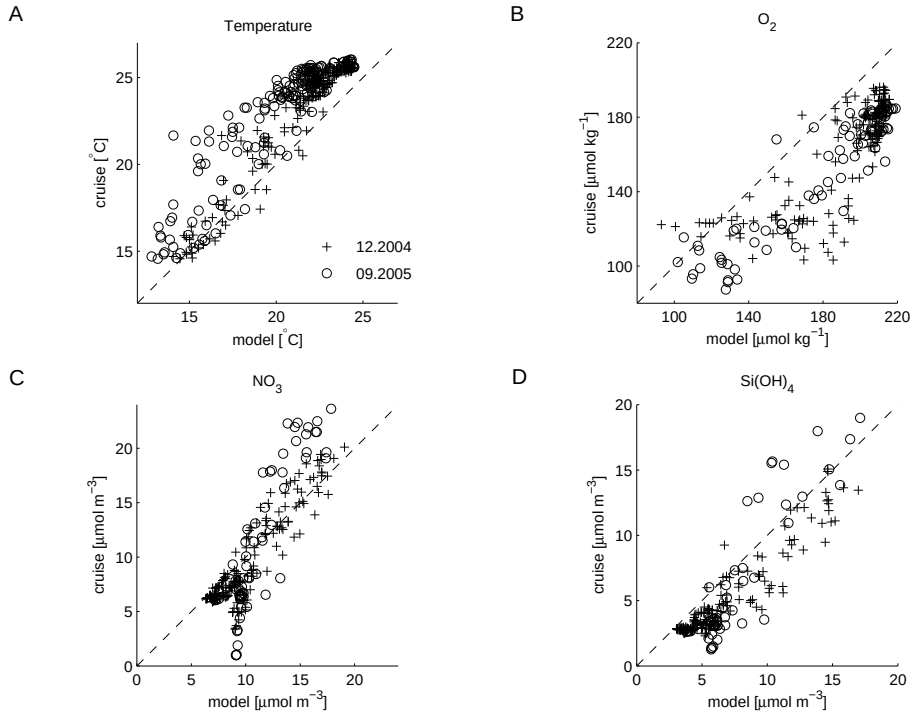

Fig. 1. Collection of scatter plots representing in situ and the modeled hydrographic conditions for the depth range of 0–150 m and along two longitude lines (140° W and 110° W). The model results are meridional averages from 1° S–1° N, and 15-day or 9-day time averages (roughly corresponding to the length of EB04 and EB05 equatorial transects). December 2004 data (+) and September 2005 (o) are plotted separately. The dashed diagonal line in each scatter plot is the 1 : 1 perfect model-data fit line. **(A)** T (°C); **(B)** O_2 (mg O_2 m^{-3}); **(C)** NO_3 (mmol N m^{-3}); **(D)** $Si(OH)_4$ (mmol Si m^{-3}).

BGD
9, 701–744, 2012

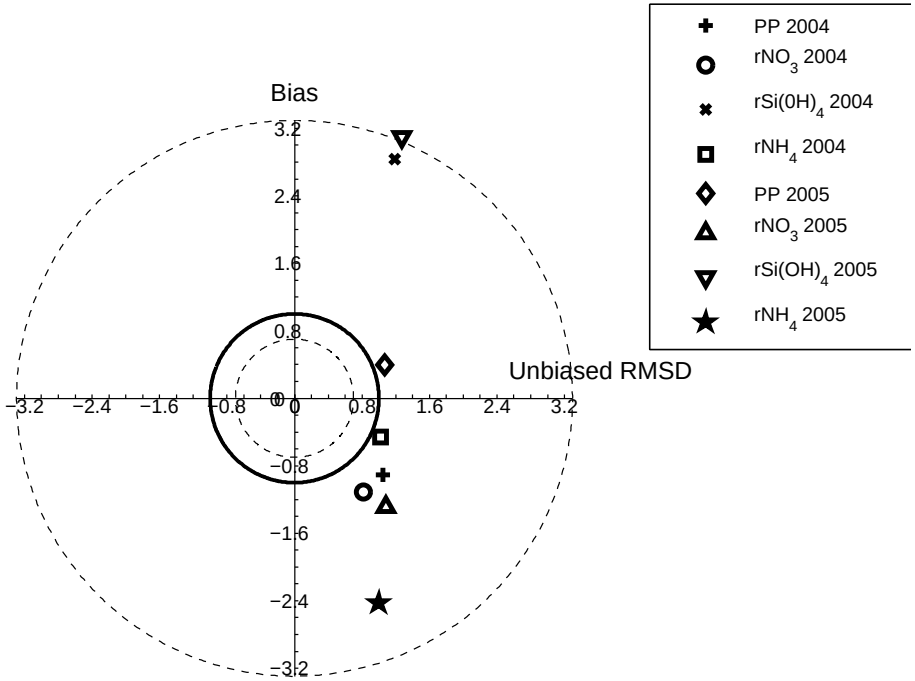

Fig. 2. Target diagram of PP and nutrient uptake rates in the EEP during 2004–2005. Diagram shows the normalized B and $RMSD_{cp}$ (unbiased $RMSD_{cp}$) for the model PP, ρNO_3, $\rho Si(OH)_4$ and ρNH_4 relative to the EB observations from December 2004 and September 2005. Concentric circles represent $RMSD_{tot}$ isolines.

BGD
9, 701–744, 2012

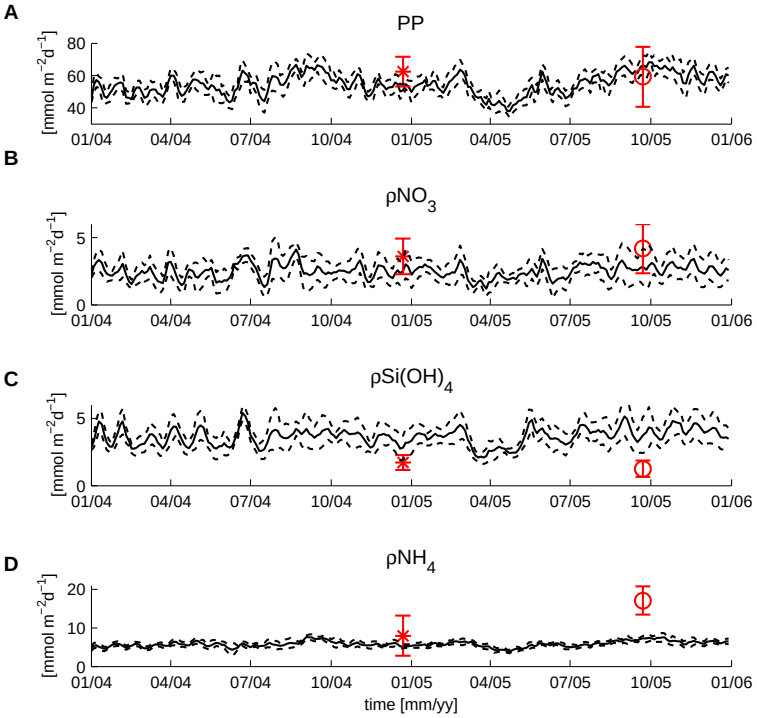

Fig. 3. Model time series of carbon and nutrient uptake rates in the EEP during 2004–2005. Results are depth-integrated and area-averaged. Solid lines are the box means and dashed lines are 1σ around the mean. Cruise data are from December 2004 (*) and September 2005 (o). Horizontal error bars on cruise estimates indicate the length of equatorial transects in days, while vertical error bars correspond to 1σ around the EEP mean. **(A)** PP (mmol C m^{-2} d^{-1}); **(B)** ρNO_3 (mmol N m^{-2} d^{-1}); **(C)** $\rho Si(OH)_4$ (mmol Si m^{-2} d^{-1}); **(D)** ρNH_4 (mmol N m^{-2} d^{-1}).

BGD
9, 701–744, 2012

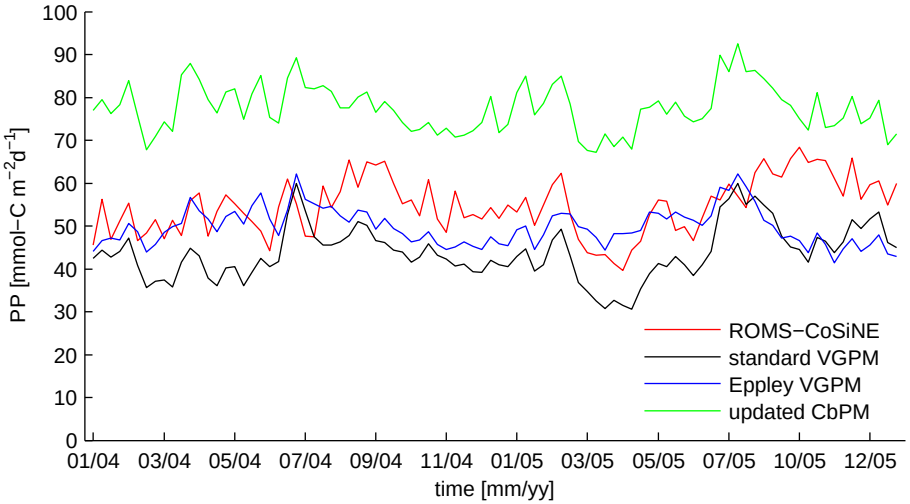

Fig. 4. Comparison of model and satellite primary productivity time series in the EEP during 2004–2005. Thick solid line is the ROMS-CoSiNE estimate. Standard VGPM result is marked with a thin solid line with open circles. The Eppley-modified VGPM result is labeled with a thin solid line with crosses. The updated CbPM result is represented by a thin solid line with asterisks. Satellite data from http://www.science.oregonstate.edu/ocean.productivity/. See text for a detailed description of satellite model PP algorithms.

BGD
9, 701–744, 2012

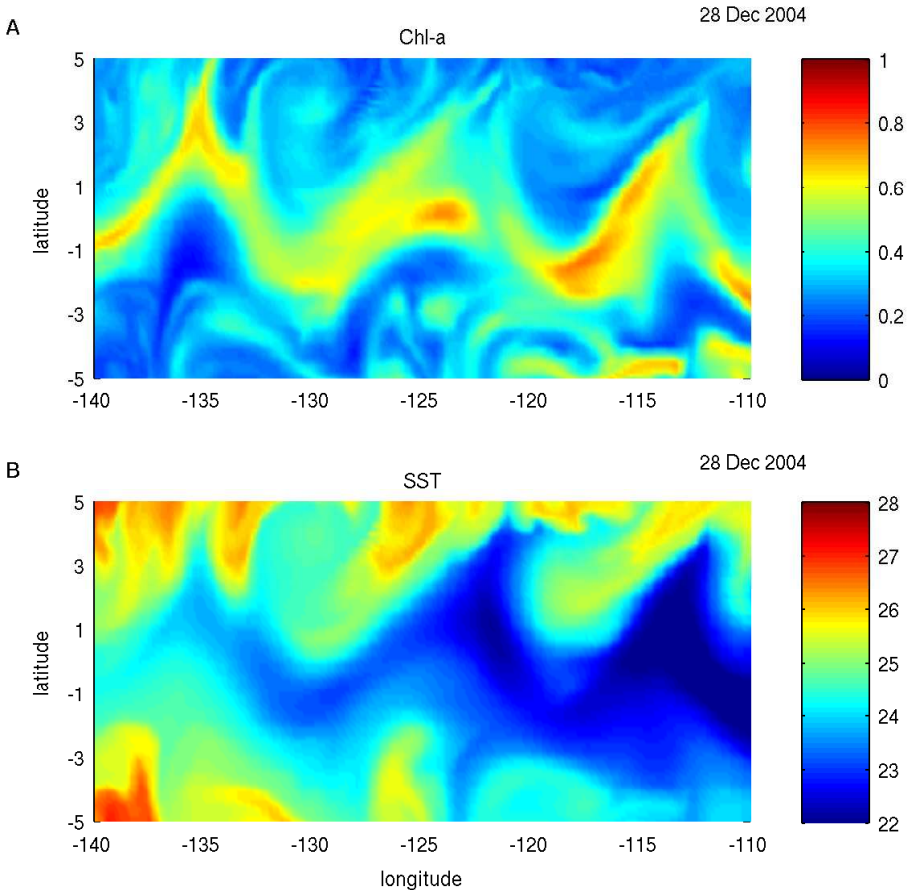

Fig. 5. An example of model detected TIW signatures in the Pacific ROMS-CoSiNE Chl-*a* and SST fields from 28 December 2004, towards the end of the along-equatorial transect during EB04. **(A)** Chl (mg Chl m^{-3}); **(B)** SST (°C).

BGD
9, 701–744, 2012

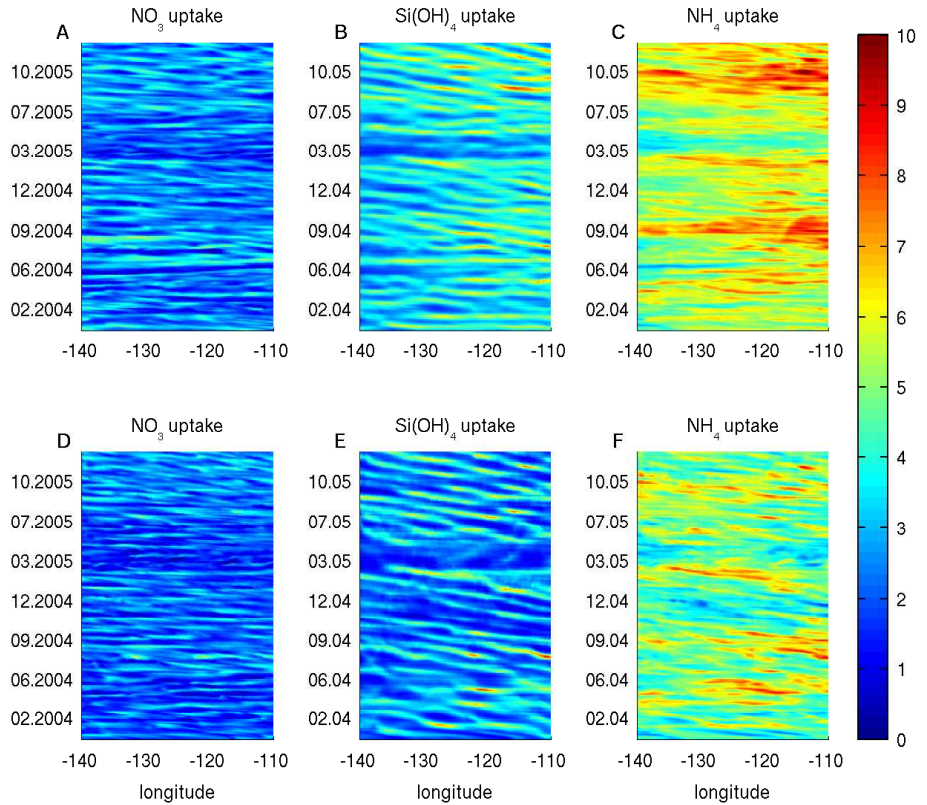

Fig. 6. Time-longitude diagrams of depth integrated and meridional average nutrient uptake rates in the EEP. Time period is from January 2004 to December 2005. Top panels **(A–C)** show nutrient uptake rates averaged over 1° S–1° N and bottom panels **(D–F)** show nutrient uptake rates averaged over 1–3° N. **(A,D)** ρNO_3 (mmol N m^{-2} d^{-1}); **(B,E)** $\rho Si(OH)_4$ (mmol Si m^{-2} d^{-1}); **(C,F)** ρNH_4 (mmol N m^{-2} d^{-1}).

BGD
9, 701–744, 2012

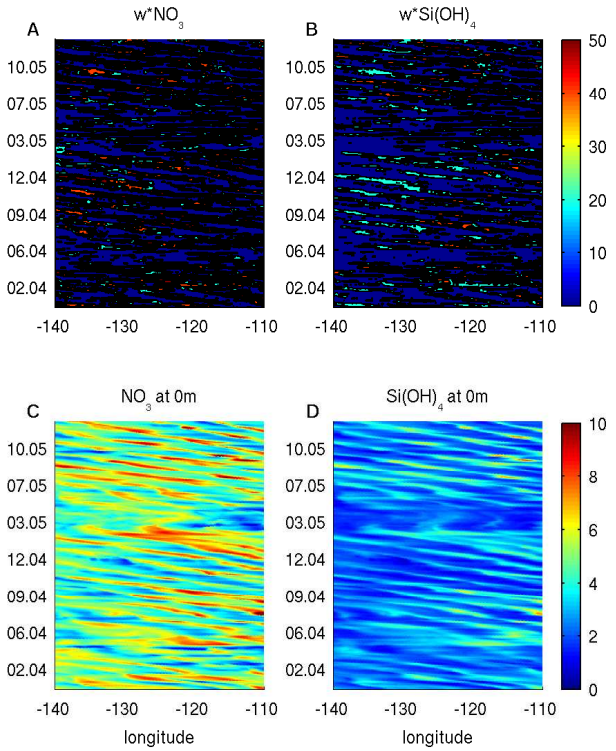

Fig. 7. Time-longitude diagrams of meridional-averaged positive nutrient supply flux and surface concentration in the EEP. Top panels **(A,B)** show positive upwelling supply flux averaged over 1–3° N, and bottom panels **(C,D)** show nutrient surface concentrations also averaged over 1–3° N. Time period is from January 2004 to December 2005. **(A)** NO_3 upwelling supply ($w * NO_3$) (mmol N m^{-2} d^{-1}); **(C)** NO_3 at 0 m (mmol N m^{-3}); **(B)** $Si(OH)_4$ upwelling supply ($w * Si(OH)_4$) (mmol Si m^{-2} d^{-1}); **(D)** $Si(OH)_4$ at 0 m (mmol Si m^{-3}).

BGD
9, 701–744, 2012

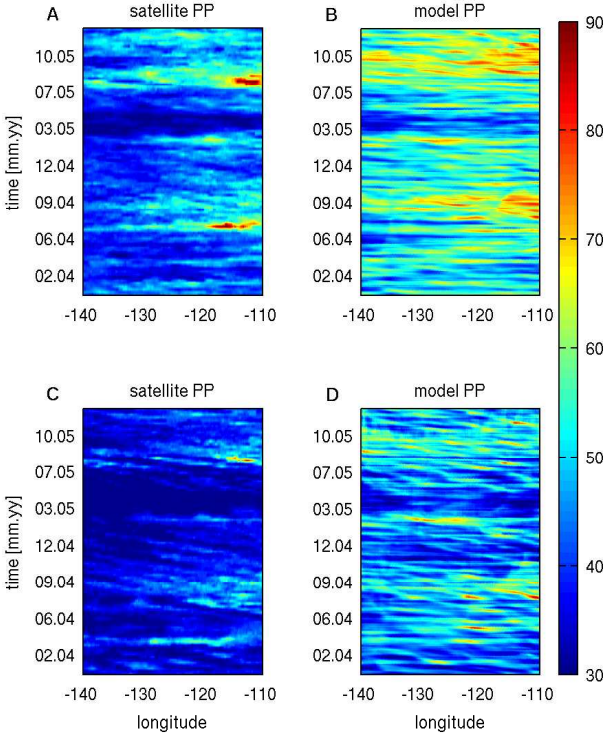

Fig. 8. Time-longitude diagrams of depth integrated and meridional average model and satellite PP in the EEP. Time period is from January 2004 to December 2005. Top panels **(A,B)** show PP averaged over 1° S–1° N and bottom panels **(C,D)** show PP averaged over 1–3° N. **(A,C)** standard VGPM satellite estimate of PP (mmol C m^{-2} d^{-1}) based on Behrenfeld and Falkowski (1997); **(B,D)** ROMS-CoSiNE PP (mmol C m^{-2} d^{-1}).

BGD
9, 701–744, 2012